Model-Based Separation, Detection, and Classification of Eye Movements

Federico Wadehn, Thilo Weber, David J. Mack, Thomas Heldt, and Hans-Andrea Loeliger

***Abstract*—*Objective:* We present a physiologically motivated eye movement analysis framework for model-based separation, detection, and classification (MBSDC) of eye movements. By estimating kinematic and neural controller signals for saccades, smooth pursuit, and fixational eye movements in a mechanistic model of the oculomotor system we are able to separate and analyze these eye movements independently. *Methods:* We extended an established oculomotor model for horizontal eye movements by neural controller signals and by a blink artifact model. To estimate kinematic (position, velocity, acceleration, forces) and neural controller signals from eye position data, we employ Kalman smoothing and sparse input estimation techniques. The estimated signals are used for detecting saccade start and end points, and for classifying the recording into saccades, smooth pursuit, fixations, post-saccadic oscillations, and blinks. *Results:* On simulated data, the reconstruction error of the velocity profiles is about half the error value obtained by the commonly employed approach of filtering and numerical differentiation. In experiments with smooth pursuit data from human subjects, we observe an accurate signal separation. In addition, in neural recordings from non-human primates, the estimated neural controller signals match the real recordings strikingly well. *Significance:* The MBSDC framework enables the analysis of multi-type eye movement recordings and provides a physiologically motivated approach to study motor commands and might aid the discovery of new digital biomarkers. *Conclusion:* The proposed framework provides a model-based approach for a wide variety of eye movement analysis tasks.**

***Index Terms*—Eye movements, Kalman filter, oculomotor system, saccades, signal separation, smooth pursuit eye movements, sparse Bayesian learning, state space models.**

I. Introduction

EYE movements provide valuable information about the visual system and related brain areas [1]. Early oculomotor studies took place in tightly controlled environments with head-fixed subjects, simple stimuli, and single-type eye movements. In contemporary mixed-type [2] and free-viewing [3] experiments, accurate estimation of eye movement parameters is more demanding. A further challenge is posed by the large variety of eye tracking technologies, which range from invasive methods such as search coils, to electro-oculography, to non-contact methods, such as infrared- and video-oculography [4], [5]. These techniques vary, among others, in their signal-to-noise ratio and sampling rates. Such diverse recordings call for robust and flexible signal analysis algorithms.

Traditionally, kinematic signals (eye position, velocity and acceleration) have been obtained by lowpass filtering and numerical differentiation of the measured eye position [6]. Unwary filtering, however, can substantially alter characteristics of eye movement recordings, in particular saccadic peak velocities [7], [8]. Nonetheless, filtered position and velocity profiles are commonly used for detecting saccades and extracting relevant parameters. Prominent approaches are the Identification by Velocity (IVT) or Dispersion Threshold (IDT) algorithms [9]. By themselves, IVT and IDT are not well-suited for multi-type recordings due to the overlap of saccades and other eye movements in the velocity domain [10]. In particular, in smooth pursuit eye movement (SPEM) analyses, naturally occurring catch-up saccades must be detected to allow for a meaningful analysis. An ad-hoc remedy is to first estimate the SPEM velocity profile by lowpass filtering and then to detect saccades using time-varying thresholds [11].

Recent machine learning approaches, trained on annotated data, classify eye position recordings directly into different types of eye movements using algorithms such as random forests [12], hidden Markov models [13], and neural networks [14]. While performant, such approaches lack a physiological basis and their estimation quality heavily depends on the training data available. Hand-labeled data, however, were shown to present substantial inter-rater variability [15], [16].

In biomechanics there has been a significant effort in mechanistic modeling of the oculomotor plant and the pertaining neural controller signals [17]–[21]. Such models have been used, among others, for obtaining biomarkers from model parameter estimates [22]. In this paper, we propose a physiological model for different types of eye movements such as saccades, smooth pursuit eye movements (SPEM), and fixational eye movements (FEM). The present model describes one-dimensional eye movements and is obtained by extending the

Manuscript received January 7, 2019; revised May 6, 2019; accepted May 17, 2019. Date of publication May 30, 2019; date of current version January 20, 2020. *(Federico Wadehn and Thilo Weber contributed equally to this work.) (Corresponding author: Federico Wadehn.)*

F. Wadehn is with the Signal and Information Processing Laboratory, ETH Zurich, 8092 Zurich, Switzerland (e-mail: wadehn@isi.ee.ethz.ch).

T. Weber and H.-A. Loeliger are with the Signal and Information Processing Laboratory, ETH Zurich.

D. J. Mack was with the University Hospital Zurich.

T. Heldt is with the Institute for Medical Engineering & Science, Massachusetts Institute of Technology.

This paper has supplementary downloadable material available at http://ieeexplore.ieee.org, provided by the authors.

Digital Object Identifier 10.1109/TBME.2019.2918986

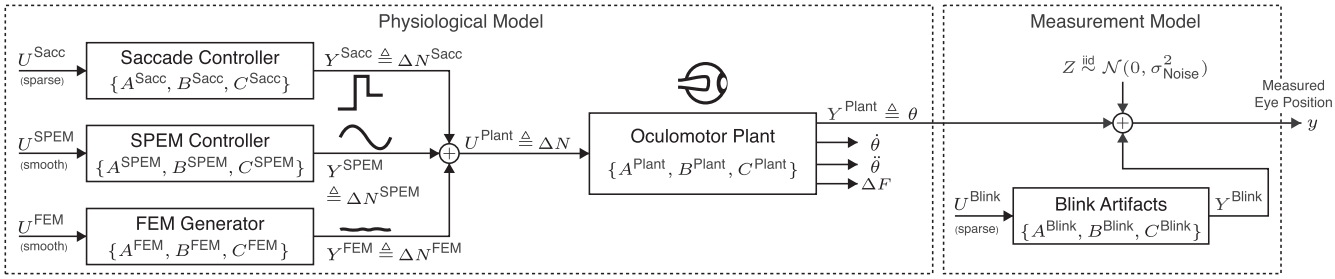

Fig. 1. Physiological and measurement model of the MBSDC framework: The three neural controller systems for saccades, SPEM, and FEM feed into the oculomotor plant, whose output (eye position θ) is fed into the measurement model. The latter accounts for measurement noise and blink artifacts, and outputs the measured eye position y.

oculomotor plant [20] for horizontal eye movements with neural controller signals for saccades, SPEM, and FEM. By combining this model with state space methods such as Gaussian message passing [23] (a generalization of Kalman filtering) and sparse input estimation [24], we obtain a unifying framework that we denote **M**odel-**B**ased Signal **S**eparation, **D**etection, and **C**lassification (**MBSDC.**[1]), for

1) estimation of kinematic signals (eye position, velocity, acceleration, and forces of oculomotor muscles),
2) estimation of neural controller signals to the oculomotor muscles from positional eye movement recordings,
3) separation and classification of eye movements,
4) extraction of relevant parameters (e.g., saccadic amplitudes, durations, and peak velocities as well as post-saccadic oscillation start/end points).

Preliminary results of this approach were presented in [25].

II. Background

Over a hundred years ago, Dodge published the first taxonomy of the five main types of eye movements [26], now commonly known as saccades, SPEM, vestibulo-ocular reflex (VOR), optokinetic nystagmus (OKN), and vergence. *Saccades* are fast eye movements for rapid gaze changes. Their characteristics are influenced, among others, by age [27], exposure to video games [28], and neurodegenerative diseases [29]. In spinocerebellar degeneration, for example, saccadic peak velocity is markedly reduced [30]. *SPEM* are slower eye movements for "following an object moving across the field of vision" [26]. The ability to perform SPEM can be affected by various disorders, among which schizophrenia [31] and autism [32]. *VOR* is a slow, compensatory eye movement for "fixation during head rotation" [26]. *OKN* is a sequence of fast and slow eye movements that stabilize the gaze during egomotion, and in *vergence* the two eyes slowly turn into opposite directions. While the eyes seem still during *fixations*, there is yet another class of eye movements subsuming microsaccades and slow fixational eye movements (FEM) below 1° of visual angle. These include tremor and drift. FEM become pronounced in, e.g., Parkinson's disease, where ocular tremor was observed in a large fraction of patients [33].

[1]Code: https://bitbucket.org/magnetilo/mbsdc_code

III. Physiological and Measurement Model

Dodge's eye movement taxonomy phenomenologically is still undisputed, but it is not reflected in the underlying neurophysiology. The neural controller system actually splits into separate subsystems in the brainstem [21], [34]: A slow subsystem responsible for SPEM, VOR, vergence and the slow phases of OKN, and a fast subsystem for generating saccades and the quick phases of OKN. Motivated by this distinction, we split the neural controller into three subsystems: one for fast, one for slow, and one for fixational eye movements. We denote these the saccade, SPEM, and FEM controllers (Fig. 1).

The complete model consists of a physiological and a measurement model (dashed boxes in Fig. 1). The physiological model is composed of the three neural controller systems and a mechanistic oculomotor plant for horizontal eye movements. The model's output Y^{Plant} represents the noise-free eye position. The signal Y^{Plant} is fed into the measurement model that accounts for measurement noise and blink artifacts. Each of these subsystems is described by a linear state space model (SSM) of the form

$$X_k^{(m)} = A^{(m)} X_{k-1}^{(m)} + B^{(m)} U_k^{(m)} \tag{1}$$

$$Y_k^{(m)} = C^{(m)} X_k^{(m)}, \tag{2}$$

with states $X^{(m)} = (X_1^{(m)}, \dots, X_L^{(m)})$, inputs $U^{(m)} = (U_1^{(m)}, \dots, U_L^{(m)})$, outputs $Y^{(m)} = (Y_1^{(m)}, \dots, Y_L^{(m)})$, and $m \in \{\text{Sacc}, \text{SPEM}, \text{FEM}, \text{Plant}, \text{Blink}\}$. The length (in samples) of the eye position time series is denoted by L. The input to the oculomotor plant is given by

$$U_k^{\text{Plant}} = Y_k^{\text{Sacc}} + Y_k^{\text{SPEM}} + Y_k^{\text{FEM}}, \tag{3}$$

i.e., the superposition of the saccadic, SPEM and FEM neural controller signals. The recorded eye position is

$$Y_k = Y_k^{\text{Plant}} + Y_k^{\text{Blink}} + Z_k, \tag{4}$$

with $Z \overset{\text{iid}}{\sim} \mathcal{N}(0, \sigma^2_{\text{Noise}})$ being an independent and identically distributed (iid) Gaussian noise signal. The signal Y^{Blink} accounts for blink artifacts. Note that we follow the convention to denote variables as uppercase when they are random quantities and lowercase when they are observed realizations. In the following, we describe each subsystem in detail.

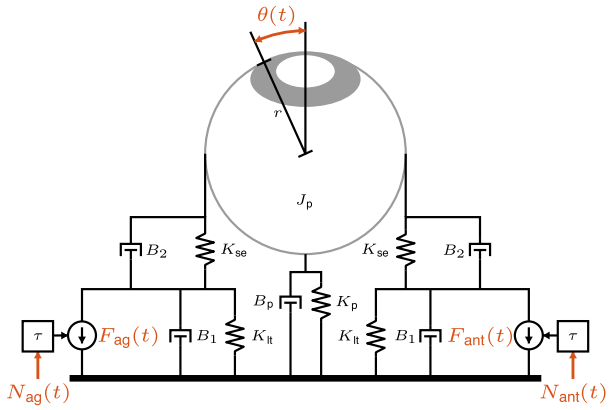

Fig. 2. Oculomotor plant for horizontal eye movements from [20]. J_p is the eye ball's moment of inertia; r is the radius of the eye globe; K_{se}, K_{lt}, B_1, and B_2 are spring and damping constants of the agonist and antagonist muscles (lateral and medial recti); K_p and B_p are the lumped spring and damping constants of the other eye muscles and supporting tissues surrounding the eye ball; and τ is the time-constant of the first-order lag system whose inputs are the neural controller signals N_{ag} and N_{ant}, and whose outputs are the active state tensions F_{ag} and F_{ant}.

A. Oculomotor Plant for Horizontal Eye Movements

In our model we used the oculomotor plant for horizontal eye movements from [20], shown in Fig. 2. This model is described by the linear differential equations

$$\dddot{\theta}(t) + R_2\ddot{\theta}(t) + R_1\dot{\theta}(t) + R_0\theta(t) = \delta\left(B_2[\dot{F}_{ag}(t) - \dot{F}_{ant}(t)] + K_{se}[F_{ag}(t) - F_{ant}(t)]\right) \quad (5)$$

$$\dot{F}_{ag}(t) = [N_{ag}(t) - F_{ag}(t)]/\tau, \quad (6)$$

$$\dot{F}_{ant}(t) = [N_{ant}(t) - F_{ant}(t)]/\tau, \quad (7)$$

where

$$\theta(t)\ [^\circ],\ \ \dot{\theta}(t)\ [^\circ/\mathrm{s}],\ \ \ddot{\theta}(t)\ [^\circ/\mathrm{s}^2] \quad (8)$$

are the one-dimensional angular eye position, velocity, and acceleration, respectively, and

$$F_{ag}(t)\ [\mathrm{N}],\ \ F_{ant}(t)\ [\mathrm{N}],\ \ N_{ag}(t)\ [\mathrm{N}],\ \ N_{ant}(t)\ [\mathrm{N}] \quad (9)$$

are the active state tensions and neural controller signals of the agonist (ag) and antagonist (ant) muscles (measured in Newtons [N] as in [18], [20]). The coefficients in (5)–(7) are

$$\delta = \frac{180}{\pi r J_p(B_1 + B_2)}, \quad (10)$$

$$R_0 = \frac{2K_{lt}K_{se} + (K_{se} + K_{lt})K_p}{J_p(B_1 + B_2)}, \quad (11)$$

$$R_1 = \frac{2B_1K_{se} + 2K_{lt}B_2 + (B_1 + B_2)K_p + (K_{se} + K_{lt})B_p}{J_p(B_1 + B_2)}, \quad (12)$$

$$R_2 = \frac{J_p(K_{se} + K_{lt}) + 2B_1B_2 + (B_1 + B_2)B_p}{J_p(B_1 + B_2)}, \quad (13)$$

where the parameters $J_p, r, B_1, K_{se}, \ldots$, are defined in Fig. 2. Note that in (5)–(7) the agonist and antagonist forces and pertaining neural controller signals appear only as differences. Therefore, it is only possible to estimate $\Delta F \triangleq F_{ag} - F_{ant}$ and $\Delta N \triangleq N_{ag} - N_{ant}$ from positional eye data. To express (5)–(7) as a continuous-time SSM (see [19], Chapter 3.6.3) we define

$$X^{\text{Plant}}(t) \triangleq (\theta(t), \dot{\theta}(t), \ddot{\theta}(t), \Delta F(t))^\mathsf{T} \quad (14)$$

$$U^{\text{Plant}}(t) \triangleq \Delta N(t). \quad (15)$$

The resulting SSM matrices are

$$\tilde{A}^{\text{Plant}} = \begin{bmatrix} 0 & 1 & 0 & 0 \\ 0 & 0 & 1 & 0 \\ -R_0 & -R_1 & -R_2 & \delta(K_{se} - \frac{B_2}{\tau}) \\ 0 & 0 & 0 & -\frac{1}{\tau} \end{bmatrix} \quad (16)$$

$$\tilde{B}^{\text{Plant}} = \begin{bmatrix} 0 & 0 & \frac{B_2}{\tau} & \frac{1}{\tau} \end{bmatrix}^\mathsf{T} \quad (17)$$

$$\tilde{C}^{\text{Plant}} = \begin{bmatrix} 1 & 0 & 0 & 0 \end{bmatrix}. \quad (18)$$

The corresponding discrete-time matrices A^{Plant}, B^{Plant} and C^{Plant} used in the following computations are obtained by a zero-order hold discretization with a data-dependent sampling period T_s (see, e.g., [35]).

The proposed one-dimensional model does not capture the complexity of vertical and in particular oblique eye movements, which are determined by the interaction of the recti and oblique muscles. As a first approximation, akin to [22], horizontal and vertical eye movements can be treated independently and the vertical component can be described with a one-dimensional model as in Fig. 2, with possibly adapted model parameters. In the case of vertical eye movements, F_{ag} and F_{ant} represent the resulting aggregate agonist and antagonist vertical forces, respectively. For signal separation and saccade detection such simplified representation suffices (see Section V-D and Fig. S3 in the Online Supplementary Material). However, such aggregation would clearly not be sufficient for neural input estimation. To capture the full complexity and to account for the fact that horizontal and vertical saccades are not independent, 3D models such as [21] could be used instead.

B. Saccade Controller

The saccadic neural controller signal

$$Y_k^{\text{Sacc}} \triangleq \Delta N_k^{\text{Sacc}}, \quad (19)$$

with $k = 1, \ldots, L$, is commonly approximated by a pulse-step signal [17], [18]. Such pulse-step signals can be modeled by a zero-order hold system with $A^{\text{Sacc}} = B^{\text{Sacc}} = C^{\text{Sacc}} = 1$, i.e.,

$$X_k^{\text{Sacc}} = X_{k-1}^{\text{Sacc}} + U_k^{\text{Sacc}} \quad (20)$$

$$Y_k^{\text{Sacc}} = X_k^{\text{Sacc}}, \quad (21)$$

with $U_k^{\text{Sacc}}, X_k^{\text{Sacc}}, Y_k^{\text{Sacc}} \in \mathbb{R}$ and $U^{\text{Sacc}} = (U_1^{\text{Sacc}}, \ldots, U_L^{\text{Sacc}})$ being a sparse input signal (i.e., $U^{\text{Sacc}} = 0$ for most entries).

1) Modeling Sparse Inputs: In Bayesian estimation, sparse inputs $U = (U_1, \ldots, U_L)$ with $U_k \in \mathbb{R}$ and $k = 1, \ldots, L$, are commonly modeled by iid sparsity-promoting priors $p(u_k)$ as described in the Appendix D. Sparse Bayesian learning [36] relies on the hierarchical representation [37]

$$p(u_k) = \sup_{\sigma_k \geq 0} \mathcal{N}(u_k|0, \sigma_k^2)p(\sigma_k), \quad (22)$$

with a suitable hyperprior $p(\sigma_k)$ (see Appendix D, (79)). Since σ_k^2 is a variance, such representations have been called *normal with unknown variances* (NUV) [24], [37]. Using this NUV representation for U_k^{Sacc}, for fixed σ_k^{Sacc}, the sparse inputs become Gaussian, i.e., $U_k^{\text{Sacc}} \sim \mathcal{N}(0, (\sigma_k^{\text{Sacc}})^2)$. Inference in SSMs driven by such Gaussian inputs can be carried out via Kalman smoothing. However, the representation (22) requires an optimization over the σ_k's. This can, e.g., be done by an expectation maximization (EM) algorithm (Section IV-A2), which alternates between a Gaussian message passing step with fixed σ_k's and an update step for the σ_k's.

2) Modeling Group Sparse Inputs: Neural recordings in non-human primates suggest that Y^{Sacc} is more accurately described by a pulse-slide-step rather than by a simple pulse-step [20], [38]. In a pulse-slide-step, the initial upstroke is followed by a transient exponential decay, before the step concludes with (usually) a precipitous drop to baseline. Figures 5(a) and 7 show examples of such pulse-slide-step controller signals. To allow shapes of Y^{Sacc} beyond pulse-steps, we assume that the inputs U^{Sacc} are group-sparse, i.e., the sparsity pattern has temporal correlations. To obtain group sparsity, we filter the estimated NUV parameters $\sigma^{\text{Sacc}} = (\sigma_1^{\text{Sacc}}, \dots, \sigma_L^{\text{Sacc}})$ with the FIR filter

$$w_k = c \cdot kT_{\text{s}} \cdot e^{-kT_{\text{s}}/\tau_w}, \; k = 1, \dots, D, \tag{23}$$

where c is a normalizing constant and D the filter length, that depends on the sampling rate T_s. Using our neural recordings, we find that suitable values of the decay rate τ_w lie between 2 and 8 ms.

C. SPEM Controller

The smooth adaptation to the target velocity during the open-loop phase of SPEM [39] suggests to model the neural SPEM controller signal

$$Y_k^{\text{SPEM}} \triangleq \Delta N_k^{\text{SPEM}} \tag{24}$$

by a first-order hold system with smooth velocity changes. This corresponds to a SSM of the form (1)–(2), with

$$A^{\text{SPEM}} = \begin{bmatrix} 1 & T_{\text{s}} \\ 0 & 1 \end{bmatrix}, B^{\text{SPEM}} = \begin{bmatrix} 0 \\ \sqrt{T_{\text{s}}} \end{bmatrix}, C^{\text{SPEM}} = \begin{bmatrix} 1 & 0 \end{bmatrix}, \tag{25}$$

with $U_k^{\text{SPEM}}, Y_k^{\text{SPEM}} \in \mathbb{R}$ and $X_k^{\text{SPEM}} \in \mathbb{R}^2$, where the velocity (second component of the state vector) is driven by a Gaussian input $U^{\text{SPEM}} \overset{\text{iid}}{\sim} \mathcal{N}(0, \sigma_{\text{SPEM}}^2)$. This model is particularly useful if the target motion is unknown.

In controlled experiments with a sinusoidal target velocity, the neural controllers can instead be modeled by the SSM

$$A^{\text{SPEM}} = \begin{bmatrix} 1 & T_{\text{s}} & 0 \\ 0 & \cos(2\pi f_{\text{Target}} T_{\text{s}}) & \sin(2\pi f_{\text{Target}} T_{\text{s}}) \\ 0 & -\sin(2\pi f_{\text{Target}} T_{\text{s}}) & \cos(2\pi f_{\text{Target}} T_{\text{s}}) \end{bmatrix}$$

$$B^{\text{SPEM}} = \begin{bmatrix} 0 & 0 \\ \sqrt{T_s} & 0 \\ 0 & \sqrt{T_s} \end{bmatrix}, \; C^{\text{SPEM}} = \begin{bmatrix} 1 & 0 & 0 \end{bmatrix}, \tag{26}$$

where f_{Target} is the frequency of the target. This SSM is driven by a two-dimensional input $U^{\text{SPEM}} \overset{\text{iid}}{\sim} \mathcal{N}(\mathbf{0}, \sigma_{\text{SPEM}}^2 \cdot I_2)$, where I_2 indicates a 2×2 identity matrix.

D. FEM Generator

FEM are small variations around the fixation target, which in our model are generated by the neural signal

$$Y_k^{\text{FEM}} \triangleq \Delta N_k^{\text{FEM}}. \tag{27}$$

This signal is modeled by a first-order lag system with $A^{\text{FEM}} = e^{-T_{\text{s}}/\tau_{\text{FEM}}}$, $B^{\text{FEM}} = \sqrt{T_{\text{s}}}$, $C^{\text{FEM}} = 1$, resulting in

$$X_k^{\text{FEM}} = e^{-T_{\text{s}}/\tau_{\text{FEM}}} \cdot X_{k-1}^{\text{FEM}} + \sqrt{T_{\text{s}}} \cdot U_k^{\text{FEM}} \tag{28}$$

$$Y_k^{\text{FEM}} = X_k^{\text{FEM}}, \tag{29}$$

with $U_k^{\text{FEM}}, X_k^{\text{FEM}}, Y_k^{\text{FEM}} \in \mathbb{R}$ and $U^{\text{FEM}} \overset{\text{iid}}{\sim} \mathcal{N}(0, \sigma_{\text{FEM}}^2)$.

E. Blink Artifact Model

The most common type of disturbance in eye movement recordings are blinks. Depending on the recording technique, these have different signatures. Here, we restrict ourselves to blinks in VOG data, which are characterized by a signal drop (Fig. 4(b)). We model the blink signal (affecting the measured eye position) by a zero-order hold system

$$X_k^{\text{Blink}} = X_{k-1}^{\text{Blink}} + U_k^{\text{Blink}} \tag{30}$$

$$Y_k^{\text{Blink}} = X_k^{\text{Blink}}, \tag{31}$$

with $A^{\text{Blink}} = B^{\text{Blink}} = C^{\text{Blink}} = 1$, $U_k^{\text{Blink}}, X_k^{\text{Blink}}, Y_k^{\text{Blink}} \in \mathbb{R}$. The inputs U^{Blink} are sparse and are modeled (akin to the saccade inputs in Section III-B) by NUVs.

F. Complete Model

The complete SSM that represents both the physiological and measurement model (Fig. 1) obtained by cascading the subsystems discussed above, is still a linear SSM of the form

$$X_k = AX_{k-1} + BU_k \tag{32}$$

$$Y_k = CX_k + Z_k, \tag{33}$$

with

$$X_k = \begin{bmatrix} X_k^{\text{Blink}} \\ X_k^{\text{Plant}} \\ X_k^{\text{Sacc}} \\ X_k^{\text{SPEM}} \\ X_k^{\text{FEM}} \end{bmatrix}, \; U_k = \begin{bmatrix} U_k^{\text{Blink}} \\ U_k^{\text{Sacc}} \\ U_k^{\text{SPEM}} \\ U_k^{\text{FEM}} \end{bmatrix} \tag{34}$$

$$A = \operatorname{diag}\left(A^{\text{Blink}}, \begin{bmatrix} A^{\text{Plant}} & B^{\text{Plant}} \cdot (C^{\text{Sacc}}, C^{\text{SPEM}}, C^{\text{FEM}}) \\ \mathbf{0} & \operatorname{diag}(A^{\text{Sacc}}, A^{\text{SPEM}}, A^{\text{FEM}}) \end{bmatrix} \right) \tag{35}$$

$$B = \begin{bmatrix} B^{\text{Blink}} & \mathbf{0} \\ \mathbf{0} & \mathbf{0} \\ \mathbf{0} & \operatorname{diag}(B^{\text{Sacc}}, B^{\text{SPEM}}, B^{\text{FEM}}) \end{bmatrix} \tag{36}$$

$$C = (C^{\text{Blink}}, C^{\text{Plant}}, \mathbf{0}), \tag{37}$$

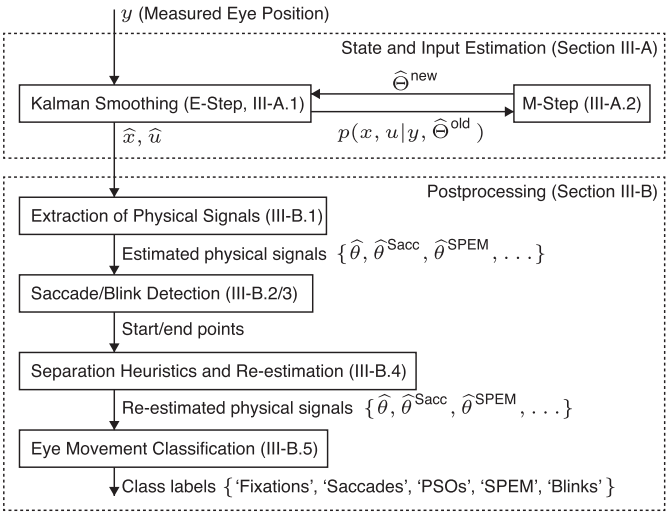

Fig. 3. Algorithmic components of the MBSDC framework.

where $\text{diag}(A, B)$ denotes the block-diagonal concatenation of the (possibly non-square) matrices A and B, and $\mathbf{0}$ is an all-zero matrix of suitable dimensions. The covariance matrices of the input U_k and the initial state X_0 are

$$\Sigma_{U_k} \triangleq \text{diag}((\sigma_k^{\text{Blink}})^2, (\sigma_k^{\text{Sacc}})^2, \sigma^2_{\text{SPEM}} \cdot I, \sigma^2_{\text{FEM}}) \tag{38}$$

$$\Sigma_{X_0} \triangleq \text{diag}(\Sigma_{X_0}^{\text{Blink}}, \Sigma_{X_0}^{\text{Plant}}, \Sigma_{X_0}^{\text{Sacc}}, \Sigma_{X_0}^{\text{SPEM}}, \Sigma_{X_0}^{\text{FEM}}). \tag{39}$$

The goal now is to estimate the states and inputs (34) from measured eye position data. This enables the recovery of kinematic and neural signals, and the separation of eye movements.

IV. Estimation

After having introduced the model, we are now ready to describe the algorithmic components of the MBSDC framework (Fig. 3). The main components are the state and input estimation steps presented in Section IV-A. The physical signals (eye position, velocity, acceleration, force, and neural controllers) are then extracted from the estimated states (Section IV-B1). These physical signals are further used to detect saccades and blinks (Sections IV-B2 and IV-B3), and for classifying the recordings into different types of eye movements (Section IV-B5). Details of the underlying estimation approach are provided in the appendices.

A. State and Input Estimation

To describe state and input estimation, we adopt a probabilistic view on SSMs. The joint density of the SSM (32)–(33) factors according to

$$p(y, x, u) = p(x_0) \prod_{k=1}^{L} p(y_k|x_k) p(x_k|x_{k-1}, u_k) p(u_k), \tag{40}$$

where the factors are given explicitly in (58). The inputs driving SPEM and FEM have iid Gaussian priors $p(u^{\text{SPEM}})$ and $p(u^{\text{FEM}})$, respectively. By contrast, the inputs triggering saccades and blinks, are equipped with sparsity-promoting priors $p(u^{\text{Sacc}})$ and $p(u^{\text{Blink}})$, represented via NUVs (22).

If all inputs were Gaussian, state and input estimation could directly be performed via Gaussian message passing [23], a generalization of Kalman smoothing (see Appendix B). However, due to the NUV representation of the sparsifying priors, the unknown NUV parameters σ^{Sacc} and σ^{Blink} have to be estimated first. The observation noise level σ_{Noise} is treated as an additional unknown parameter that needs to be estimated. Learning unknown parameters in SSMs can be performed via the EM-algorithm (Appendix D), where the E-step boils down to Kalman smoothing and the M-step has closed-form updates for the unknown parameters as described below.

1) Kalman Smoothing: For fixed input variances, the posterior distributions of the state X_k and the input U_k with $k = 1, \dots, L$, given the data $y = (y_1, \dots, y_L)$, are

$$p(x_k|y) = \mathcal{N}(x_k|m_{X_k}, V_{X_k}) \tag{41}$$

$$p(u_k|y) = \mathcal{N}(u_k|m_{U_k}, V_{U_k}). \tag{42}$$

The mean vectors (m_{X_k} and m_{U_k}) and covariance matrices (V_{X_k} and V_{U_k}) are recursively updated using the approach detailed in Appendix B. The state and input trajectory estimates are obtained from the respective means $\widehat{x} = m_X$ and $\widehat{u} = m_U$.

2) M-Step of the EM Algorithm: The unknown parameters

$$\Theta = \{\sigma_1^{\text{Sacc}}, \dots, \sigma_L^{\text{Sacc}}, \sigma_1^{\text{Blink}}, \dots, \sigma_L^{\text{Blink}}, \sigma_{\text{Noise}}\}, \tag{43}$$

are iteratively updated by an EM-algorithm. At each iteration the NUV parameters σ^{Sacc} and σ^{Blink} are updated according to

$$(\widehat{\sigma}_k^{(m),\text{new}})^2 = \frac{\mathsf{E}[(U_k^{(m)})^2|y, \widehat{\Theta}^{\text{old}}] + 2\beta^{(m)}}{2\alpha^{(m)} + 1}, \tag{44}$$

with $k \in \{1, \dots, L\}$, $m \in \{\text{Sacc}, \text{Blink}\}$. The second moments

$$\mathsf{E}[(U_k^{(m)})^2|y, \widehat{\Theta}^{\text{old}}] = V_{U_k^{(m)}} + m^2_{U_k^{(m)}} \tag{45}$$

are computed from the means and variances in (42). Appendices VII-D and VII-E discuss how the hyperparameters $\alpha^{(m)} \geq 0$ and $\beta^{(m)} \geq 0$ are chosen.

Similarly, at each EM-iteration, the observation noise level is updated according to

$$(\widehat{\sigma}_{\text{Noise}}^{\text{new}})^2 = \frac{\frac{1}{L}\sum_{k=1}^{L} \mathsf{E}[Z_k^2|y, \widehat{\Theta}^{\text{old}}]}{2\alpha_{\text{Noise}} + 1}, \tag{46}$$

where the second moment

$$\mathsf{E}[Z_k^2|y, \widehat{\Theta}^{\text{old}}] = y_k^2 - 2y_k C m_{X_k} + C(V_{X_k} + m_{X_k} m_{X_k}^{\mathsf{T}})C^{\mathsf{T}}, \tag{47}$$

is computed using the means and variances of the posterior distribution (41). The choice of the hyperparameter $\alpha_{\text{Noise}} \geq 0$ is described in Appendix E.

B. Postprocessing

Here we describe how to extract the physical signals from the estimated states $\widehat{x}$ and how to use these for saccade detection and for eye movement classification. In addition, we propose a heuristic for improving the signal separation.

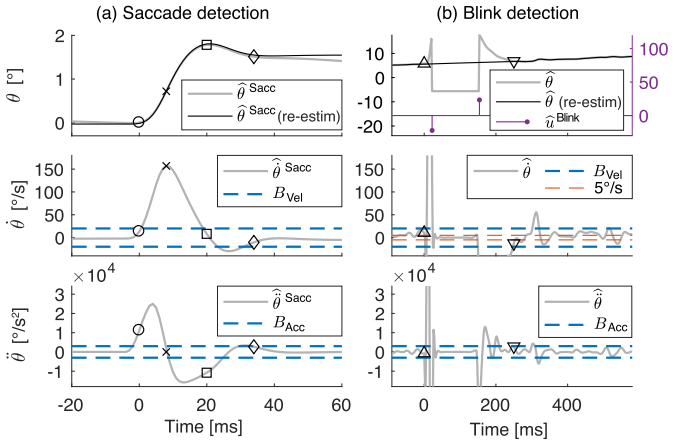

Fig. 4. (a) Detection of saccade start/end, PSO-end and peak velocity locations, marked by ◯, □, ◊, ×, respectively, and (b) detection of blink start/end locations, marked by △, ▽. The estimated eye position, velocity and acceleration profiles used for detection are shown in gray. The respective detection thresholds B_{Vel} and B_{Acc} are shown in blue. In addition, the top plot shows the re-estimated eye positions after (a) the separation heuristic described in Section IV-B4 and (b) the signal interpolation described in Section IV-B3.

1) Extracting Physical Signals: The kinematic signals

$$\widehat{\theta},\ \widehat{\dot{\theta}},\ \widehat{\ddot{\theta}},\ \widehat{\Delta F}, \tag{48}$$

the saccadic, SPEM and FEM neural controller signals

$$\widehat{\Delta N}^{\text{Sacc}},\ \widehat{\Delta N}^{\text{SPEM}},\ \widehat{\Delta N}^{\text{FEM}}, \tag{49}$$

and the estimated blink artifact signal $\widehat{y}^{\text{Blink}}$ can be read out directly from the estimated state trajectory $\widehat{x}$ (Eqns. (14), (19), (24), (27), (34)). The saccadic kinematic signals

$$\widehat{\theta}^{\text{Sacc}},\ \widehat{\dot{\theta}}^{\text{Sacc}},\ \widehat{\ddot{\theta}}^{\text{Sacc}},\ \widehat{\Delta F}^{\text{Sacc}} \tag{50}$$

are obtained by simulating the state response of the oculomotor plant to the estimated input $\widehat{\Delta N}^{\text{Sacc}}$. Similarly, the separated SPEM and FEM signals

$$\widehat{\theta}^{\text{SPEM}},\ \widehat{\dot{\theta}}^{\text{SPEM}},\ \widehat{\ddot{\theta}}^{\text{SPEM}},\ \widehat{\Delta F}^{\text{SPEM}}, \tag{51}$$

$$\widehat{\theta}^{\text{FEM}},\ \widehat{\dot{\theta}}^{\text{FEM}},\ \widehat{\ddot{\theta}}^{\text{FEM}},\ \widehat{\Delta F}^{\text{FEM}}, \tag{52}$$

are obtained by simulating the state response of the oculomotor plant to the inputs $\widehat{\Delta N}^{\text{SPEM}}$ and $\widehat{\Delta N}^{\text{FEM}}$, respectively.

2) Saccade Detection: Given the estimated saccadic velocity $\widehat{\dot{\theta}}^{\text{Sacc}}$ and acceleration profiles $\widehat{\ddot{\theta}}^{\text{Sacc}}$, we are in a position to detect saccade start/end, post-saccadic oscillation (PSO) end as well as peak-velocities. This is done using an IVT-like approach based on fixed velocity (B_{Vel}) and acceleration (B_{Acc}) thresholds. For this, we proceed as follows (Fig. 4(a)): First, we detect by a local search all peaks in $\widehat{\dot{\theta}}^{\text{Sacc}}$ that have magnitudes ranging from $20^\circ/s$ to $1000^\circ/s$. These are candidate saccadic peak velocities. Considering only time indices preceding a detected peak, we define the corresponding saccade's start point as the sample closest to the peak location for which $|\widehat{\dot{\theta}}^{\text{Sacc}}| < B_{\text{Vel}}$. Similarly, considering only time indices following a detected peak, we define the first index for which $|\widehat{\dot{\theta}}^{\text{Sacc}}| < B_{\text{Vel}}$, as the saccade's end point. The first index for which $|\widehat{\dot{\theta}}^{\text{Sacc}}| < B_{\text{Vel}}$ and $|\widehat{\ddot{\theta}}^{\text{Sacc}}| < B_{\text{Acc}}$ determines the PSO-end point. Note that there are potentially multiple velocity peaks between the start of a saccade and the PSO-end point. If this is the case, the saccade's peak velocity is chosen as the one with the largest magnitude.

3) Blink Detection and Interpolation: In VOG recordings, blinks are typically characterized by either abrupt signal drops (Fig. 4(b), top) or by velocities outside the physiological range, e.g., velocities $> 1000^\circ$/s. Signal drops are captured by the sparse input signal U^{Blink}. In this case, blinks are located by searching for non-zero entries in U^{Blink}. Non-zero entries are then assigned to the same blink if the velocity magnitude between these stays within a narrow band of 5°/s. In contrast, blinks that do not manifest themselves by an abrupt signal drop, are located by searching for velocity magnitudes $> 1000^\circ$/s. In both cases the final blink start and end points are determined following the same procedure as for the detection of PSO-end points, using fixed thresholds B_{Vel} and B_{Acc} (Fig. 4(b), center and bottom). After the blinks have been detected, the physical signals are re-estimated with the observation noise level σ_{Noise} set to some large value during the blink (Fig. 4(b), top). Eye movements during blinks are thereby smoothly interpolated by the physiological model.

4) Separation Heuristic and Re-Estimation: In SPEM-free recordings, the eye position should not change between a PSO-end point and the starting point of the following saccade. In practice, however, we observe that these points are not always aligned in our estimates. This suggests that the saccadic signals in (50) contain some amount of SPEM. The described position offsets are therefore corrected by adjusting the last non-zero input of $\widehat{u}^{\text{Sacc}}$ in the affected saccades. Signal separation can be further improved by setting to zero all entries of $\widehat{u}^{\text{Sacc}}$, that are not part of a saccade. Such spurious inputs can occur during blinks, or in saccades whose peak velocity is smaller than 20°/s (Section IV-B2). After these two post-processing steps, states and inputs are re-estimated by Kalman smoothing (Section IV-A1) with fixed inputs $\widehat{u}^{\text{Sacc}}$, and the physical signals are extracted anew (Section IV-B1), see Fig. 4(a) top.

5) Eye Movement Classification: First, we label all 'Saccades', 'PSOs', and 'Blinks' in the recording using the detected saccade and blink start/end points (Sections IV-B2 and IV-B3). The remaining samples are classified as 'SPEM' if the SPEM velocity $|\widehat{\dot{\theta}}^{\text{SPEM}}| > 1^\circ/\text{s}$, otherwise they are classified as 'Fixations'. Note that with the estimated physical signals (48)–(52) at hand, more sophisticated classification algorithms, e.g., with adaptive thresholds [40] could be used.

V. Results

We evaluated the MBSDC framework both qualitatively and quantitatively on synthetic, human, and non-human primate data. All data acquisition procedures followed the guidelines set by the National Institutes of Health and national law, and were approved by local ethics committees. In the following, we give illustrative examples for the estimation of physical signals

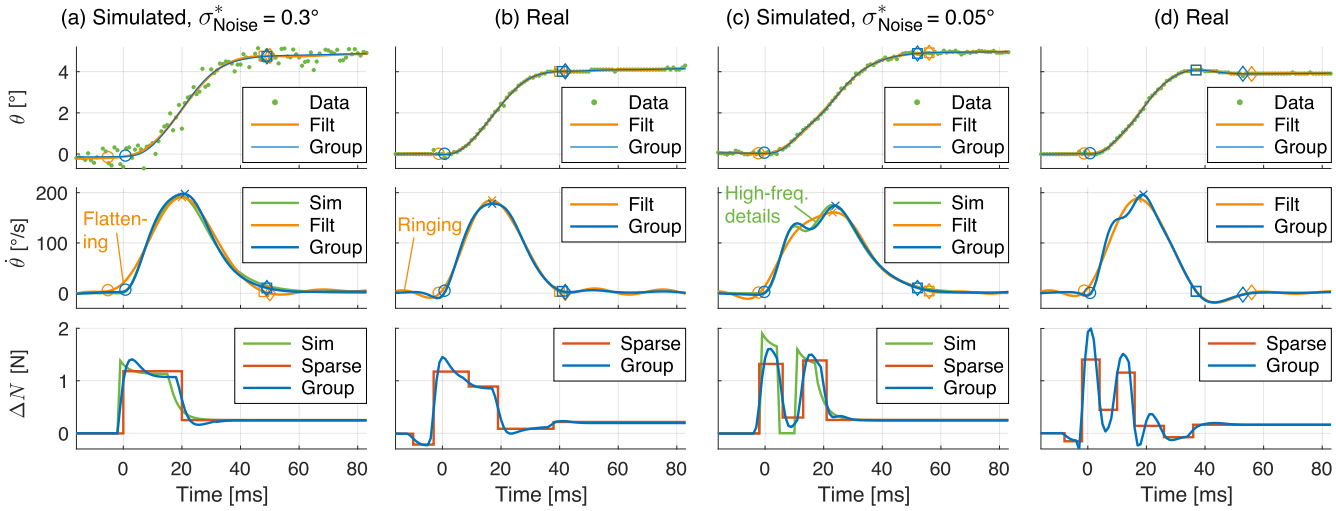

Fig. 5. (a) and (c) Simulated (Sim) eye position, velocity and neural controller signals, and corresponding estimates obtained from noisy horizontal eye position data. The position and velocity estimates are obtained by group sparse estimation (Group) and by lowpass filtering and numerical differentiation (Filt). The detected saccade start/end, PSO-end and peak velocity locations are marked by ◯, □, ◊, and ×. The bottom row shows the recovered neural input using sparse (Sparse) and group sparse input estimation. The neural controller signals cannot be estimated with the filtering approach. Note that the neural controller signal in (c) consists of two consecutive pulses, which are correctly recovered. (b) and (d) Real saccades (during SPEM) with similar shapes to (a) and (c), together with estimated physical signals and pertaining saccade markers.

in simulated and real saccade data (Section V-A2), neural controller signals in non-human primate data(Section V-B), and SPEM in human data (Section V-C). We furthermore quantitatively evaluate the MBSDC framework's ability to recover kinematic signals and detect saccades in simulated data (Sections V-A3, V-A4, and V-A5) as well as its classification performance using hand-labeled recordings (Section V-D).

A. Saccade Detection and Kinematic Signal Estimation

We simulated saccades with amplitudes of 0.6°, 1.2°, 2.5°, 5°, 10°, and 20° using the oculomotor plant described in Section III-A and synthetic pulse-slide-step neural controller signals. The pulse-slide-steps were constructed using pulse heights and widths for horizontal saccades reported in [20], that were slightly adapted such that the simulated saccades followed exactly the amplitude-velocity main sequence reported in [6]. For the quantitative evaluations in Sections V-A3, V-A4, and V-A5, we simulated 100 saccades for each amplitude at a sampling rate of 1 kHz and added white Gaussian noise with varying noise levels to these signals.

1) Evaluation Setup: We recovered the physical signals both with sparse ('Sparse') and group-sparse ('Group') input estimation of saccadic controller signals (Sections III-B1 and III-B2). We used $\sigma_{\text{SPEM}} = 0$ N/s^2, $\sigma_{\text{FEM}} = 0.2$ N/s, $\alpha_{\text{Noise}} = 0.5$, and $\alpha_{\text{Sacc}} = 0.4$ (see Appendix E). To evaluate the estimation performance of our approach, we also estimated the eye position and velocity profiles by the traditional approach of lowpass filtering and numerical differentiation (denoted by 'Filt'). We set the cutoff frequency and filter order following [8], where these values are chosen such that the peak-velocity is optimally recovered.

2) Estimation of Saccade Parameters: Figure 5(a) shows a simulated horizontal 5° saccade and the estimated position, velocity, and neural controller signals and Fig. 5(b) shows a real horizontal saccade with a similar morphology. We observe that lowpass filtering flattens the steep rising flank of the saccade and causes ringing artifacts around the saccades. These problems are not present in the MBSDC estimates. Figure 5(c) shows a simulated saccade that we generated by two consecutive pulses in the neural controller signal. The MBSDC approach is able to correctly recover these two pulses and consequently the bimodal velocity shape is correctly reconstructed, whereas in the filtering approach such details are easily lost. In our analysis, the saccadic controller signal estimated from some experimental saccade recordings consisted of two consecutive neural pulses (Fig. 5(d) and Online Supplementary Material Fig. S1), which resemble the "overlapping saccades" described in Bahill *et al.* [41].

TABLE I
ESTIMATION AND DETECTION ACCURACY OF SACCADES

	$\sigma^*_{\text{Noise}} = 0.01°$			$\sigma^*_{\text{Noise}} = 0.1°$			$\sigma^*_{\text{Noise}} = 1°$		
Estimation method	Sparse	Group	Filt	Sparse	Group	Filt	Sparse	Group	Filt
RMSE Pos. $\times 10^{-2}$	**0.29**	**0.29**	0.42	2.17	**1.93**	2.98	28.6	26.2	**23.6**
RMSE Vel.	0.62	**0.58**	1.34	2.89	**2.41**	5.23	15.3	**13.3**	25.0
Prec./Rec. 0.6°	1/1	1/1	1/1	1/0.62	1/0.63	1/0.75	1/0	1/0	1/0
Prec./Rec. 1.2°	1/1	1/1	1/1	1/1	1/1	1/1	1/0.01	1/0.02	1/0.03
Prec./Rec. 2.5°	1/1	1/1	1/1	1/1	1/1	1/1	1/0.49	1/0.70	1/0.59
Prec./Rec. 5°	1/1	1/1	1/1	1/1	1/1	1/1	1/1	1/1	1/1

Upper part: RMSE of estimated position and velocity profiles, averaged over all simulated saccades (6 different amplitudes, 100 saccades per amplitude). Bold font marks the best-performing method. *Lower part:* Precision (Prec.) and recall (Rec.) of saccade detection, shown for each amplitude separately. To compare the algorithms, in the lowpass filtering approach the peak velocity threshold for saccade detection was adapted to the noise level to yield a precision of 1.

3) Estimation Accuracy on Simulated Data: Table I shows the reconstruction accuracy of the MBSDC ('Sparse' and 'Group' sparse) and 'Filt' approaches in terms of the root mean

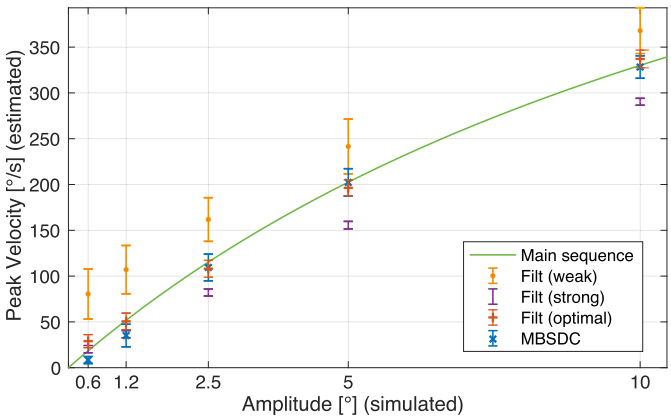

Fig. 6. Amplitude vs peak-velocity main sequence. Estimated saccadic peak velocities obtained from the MBSDC framework and by lowpass filtering. Three different lowpass filters with cutoff frequencies of 80 Hz *(weak)*, 35 Hz *(optimal)*, and 20 Hz *(strong)* were used. We simulated saccades with six different amplitudes ranging from 0.6° to about 10° that followed the main sequence characteristics described in [6], and added observation noise with $\sigma^*_{\text{Noise}} = 0.3°$. For estimated main sequences (amplitude vs peak-velocity and amplitude vs duration) using real data, see Online Supplementary Material Fig. S2.

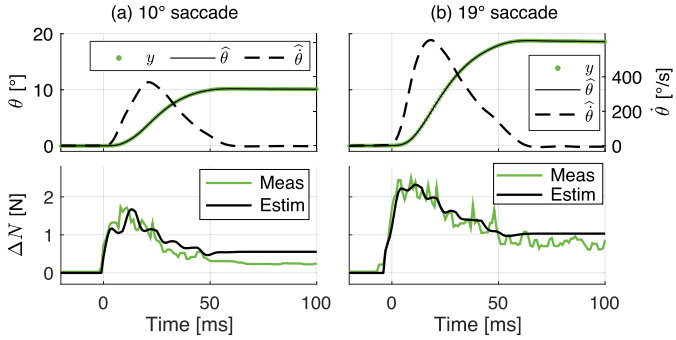

Fig. 7. *Top:* Eye movement data from a rhesus monkey performing (a) a 10° saccade and (b) a 19° saccade, together with estimated position and velocity profiles. *Bottom:* Neural firing rate measured in a single abducens neuron, and estimated neural controller signals. Position and neural recordings were averaged over 10 runs. The neural firing rate recordings are shifted 4 ms to the right and scaled in amplitude to fit the size of the estimated neural controller signal.

squared error (RMSE) of the recovered position and velocity signals. Position and, in particular, velocity profiles estimated with the MBSDC framework have lower RMSEs compared to the filtering approach. We observe that group sparse input estimation achieves slightly lower RMSEs than regular sparse input estimation.

4) Detection Performance: The lower part of Table I compares the MBSDC and filtering approach with respect to

$$\text{precision} = \frac{\#\text{ correctly detected saccades}}{\#\text{ detected saccades}}, \tag{53}$$

and

$$\text{recall} = \frac{\#\text{ correctly detected saccades}}{\#\text{ simulated saccades}}, \tag{54}$$

for simulated saccades with 0.6°, 1.2°, 2.5° and 5° amplitudes. For small observation noise ($\sigma^*_{\text{Noise}} = 0.01°$), all saccades are detected correctly. With increasing observation noise, small saccades start being missed, resulting in lower recall values.

5) Peak-Velocity Accuracy: Fig. 6 shows the amplitude-velocity main sequence extracted from simulated saccades (observation noise level $\sigma^*_{\text{Noise}} = 0.3°/\text{s}$) using the MBSDC and the lowpass filtering estimates. The accuracy of the MBSDC framework is practically on par with lowpass filtering with peak-velocity optimized parameters from [8]. Note that choosing larger (or lower) cutoff frequencies of the lowpass filter results in overestimation (or underestimation) of the peak-velocity. The accuracy of the MBSDC approach for very small saccades is slightly worse than the optimal filter, which is due to some small saccades being missed (Table I).

B. Estimation of Neural Controller Signals

We used saccade and neural data from [42] to evaluate the quality of the estimated neural controller signals. This data consists of synchronized recordings of horizontal eye positions (search coil, sampling rate 1 kHz) and neural firing rates in single abducens neurons recorded with tungsten microelectrodes in rhesus monkeys. The neural controller signal ΔN was estimated using the oculomotor plant parameters for rhesus monkeys reported in [20]. As shown in Fig. 7 the shape of the estimated neural controller signals coincide strikingly well with the neural recordings.

C. Signal Separation in Sinusoidal SPEM Data

To evaluate the accuracy of the signal separation we used eye position recordings from subjects observing a horizontally moving dot with a sinusoidal velocity profile [43]. These recordings were obtained with a limbus tracker (Skalar IRIS, Skalar Medical B.V., Delft, Netherlands) at a sampling rate of 1 kHz. The physical signals were estimated using the first-order hold model (25) with $\sigma_{\text{SPEM}} = 1\ \text{N/s}^2$, $\sigma_{\text{FEM}} = 0.2\ \text{N/s}$, $\alpha_{\text{Noise}} = 0.5$, and $\alpha_{\text{Sacc}} = 0.5$. The separated signals are shown in Fig. 8. As an alternative to the first-order hold model, one can use the sinusoidal velocity model (26). This leads to comparable separation results, but has the advantage that additional parameters such as the amplitude and the phase of the estimated SPEM velocity profile can easily be extracted (Fig. 9). These parameters might be useful for assessing the SPEM performance of test subjects which is indicative for certain neurological pathologies.

D. Classification Performance on Annotated Data

We used the annotated dataset described in [40] that was employed as ground truth for the comparison of different eye movement detection algorithms in [45]. The data were recorded at 500 Hz using the iView X Hi-Speed 1250 eye tracker (Senso-Motoric Instruments, Berlin, Germany). This dataset contains both horizontal and vertical eye position recordings from test subjects looking at images (‘Images’), vertically moving dots (‘Dots’) with constant velocity profiles, and videos (‘Videos’). Each recording is furthermore equipped with sample-by-sample labels (‘Fixations’, ‘Saccades’, ‘PSOs’, ‘SPEM’, ‘Blinks’, and

TABLE II
COHEN'S κ EVALUATED ON ANNOTATED EYE MOVEMENT DATA

	Fixations			Saccades			PSOs			SPEMs		Blinks		
Algorithm	Images	Dots	Videos	Images	Dots	Videos	Images	Dots	Videos	Dots	Videos	Images	Dots	Videos
MBSDC	0.79	0.39	**0.35**	0.87	**0.77**	**0.83**	0.65	0.48	**0.63**	**0.58**	**0.36**	0.88	0.65	0.90
IVT	0.67	0.03	0.13	0.75	0.63	0.76	–	–	–	–	–	–	–	–
LNS	–	–	–	0.81	0.75	0.81	0.64	**0.59**	**0.63**	–	–			
NSLR-HMM	0.49	**0.42**	0.29	0.72	0.67	0.71	0.52	0.38	0.47	0.49	0.26	–	–	–
IRF	**0.85**			**0.91**			**0.70**			–	–			
Human	0.92	0.84	0.82	0.95	0.91	0.94	0.88	0.82	0.83					

Evaluation of different eye movement classification algorithms. 'IVT' with fixed threshold (evaluated in [45]); 'LNS': Adaptive threshold algorithm from [40] (evaluated in [45]); 'NSLR-HMM': Hidden Markov model approach using manually engineered features [12]; 'IRF': Supervised classification algorithm using random forests [13]; 'Human': Inter-rater agreement between two eye movement experts [45]. Bold font marks the best-performing method. Entries are left empty if the evaluation is not provided in the corresponding references and marked with a dash if the algorithm is not able to perform a specific classification task.

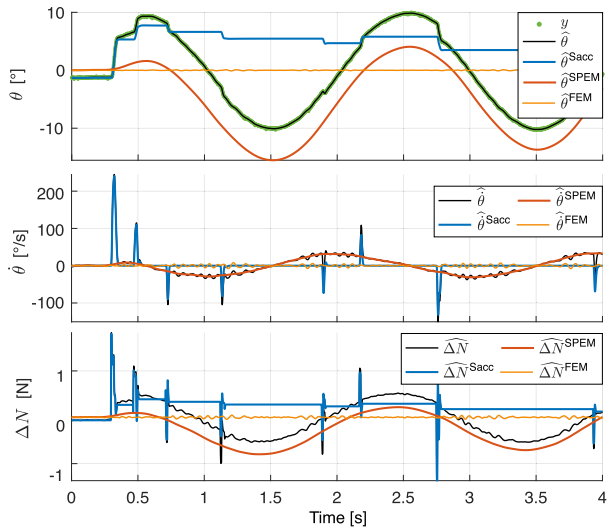

Fig. 8. Eye movement recording from a test subject tracking a horizontally moving dot with a sinusoidal velocity profile, and estimated physical signals. Note that the FEM signal is stronger during the fast SPEM phases (around time = 1, 2, and 3 s), which hints to signal-dependent noise affecting motor commands [44].

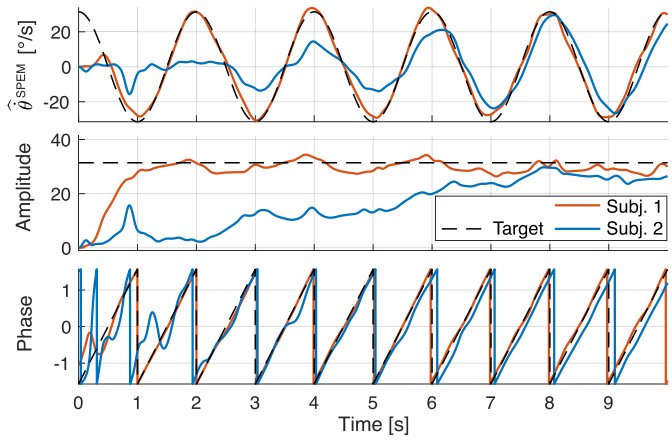

Fig. 9. *Top:* Estimated SPEM velocity profiles $\widehat{\theta}^{\text{SPEM}}$ (using model (26)) of a trained (Subj. 1) and a naive (Subj. 2) subject both observing the same moving target as in Fig. 8. *Middle and bottom:* Amplitude and phase of the estimated SPEM velocity profiles. Note that the tracking performance differs strongly between subjects.

'Unknown') annotated by two different eye movement experts. We analyzed horizontal and vertical eye movements independently. The physical signals in the horizontal eye movement recordings are estimated using the first-order hold model (25) with $\sigma_{\text{SPEM}} = 0.5\,\text{N/s}^2$, $\sigma_{\text{FEM}} = 0.8\,\text{N/s}$, $\alpha_{\text{Noise}} = 0$, and $\alpha_{\text{Sacc}} = 1$. For vertical eye movements we used the same model as for horizontal eye movements (see Section III-A and Online Supplementary Material Fig. S3). After classifying each channel, we merged the classification according to the following prioritization: 1. Blinks, 2. Saccades, 3. PSOs, 4. SPEM, 5. Fixations. For example, if a sample in the horizontal channel is labeled as a saccade and in the vertical as a fixation, the final class label is 'Saccades'. As in [45], we compared the inter-rater agreement of our classification with the manual annotations using Cohen's κ; see Table II.

VI. DISCUSSION

In the following, we discuss strengths and weaknesses of the MBSDC approach as well as potential clinical use cases.

A. Signal Separation and Classification

A novelty of the MBSDC framework is its ability to separate multi-type eye movements into their components. This allows for an independent analysis of saccades, SPEM, and FEM, each of which can provide valuable biomarkers for a number of neurological disorders [29]–[31]. For instance, the proposed SPEM parameters, phase and amplitude (Fig. 9) can be used to quantify SPEM performance, which is impaired in, e.g., schizophrenia [46]. The SPEM accuracy, often measured as gain in the closed-loop phase, can now be measured instantaneously, and the "time-to-target gain", e.g., when the amplitude reaches 95% of the target amplitude, may provide an alternative latency measure in SPEM trials. Neuromuscular disorders such as Parkinson's disease can manifest themselves via ocular tremor [33]. Hence, the estimated FEM signal intensity could serve as a quantitative digital biomarker to aid in differential diagnosis and tracking of disease progression. The estimated FEM signal is furthermore interesting for the study of motor commands. As observed in Fig. 8 the FEM component is stronger during fast SPEM phases, which is in line with the observation

that the noise affecting motor commands is dependent on the neural signal intensity [44].

Eye movement classification with the MBSDC framework is fully unsupervised and uses a very rudimentary classification scheme (Section IV-B5). Nonetheless it is only slightly worse than the random forest approach of [13] that is specifically tailored to the evaluated data set.

B. Estimation of Kinematic and Neural Controller Signals

We observe that the kinematic signals estimated by the MBSDC approach are more accurate than the ones obtained with the conventional approach of lowpass filtering and numerical differentiation. In particular, in the filtering approach finding a suitable cutoff frequency that does not affect the estimated peak velocity, but still suppresses noise, is challenging [8]. In addition, the overlap of SPEM and saccades in the frequency domain further hampers frequency domain approaches. By contrast, the MBSDC approach is an adaptive filter with no inherent cutoff frequency and is therefore able to restore high-frequency details while suppressing noise (Section V-A3).

For estimation, saccadic neural controller signals have traditionally been described by a set of parameters (e.g., pulse start, height, width and exponential decay rates) that are determined from isolated saccades [17], [18], [20], [22]. By contrast, the MBSDC framework does not use such strict modeling assumptions and is therefore capable of estimating complex saccadic neural controller signal shapes and in particular double pulses which have also been called "overlapping saccades" [41]. It remains to be investigated if such consecutive neural pulses are an artifact of our possibly underconstrained saccade model or if such consecutive pulses are also present in the pertaining neurophysiological recordings.

C. Limitations

The lack of constraints on the saccadic neural controller signals comes also with limitations: Prior knowledge on the positive correlation between neural pulse-widths and pulse-heights [47] during saccades is not encoded in our model. Encoding this into our model would increase its physiological realism and in addition might provide the necessary constraints for estimating jointly the oculomotor plant parameters and the neural controller signals, e.g., using suitable EM-updates for the model parameters akin to the updates in Section IV-A2. Without constraints, we observe that due to the flexibility of the saccadic neural controller signal such joint estimation does not provide satisfactory results. Being able to estimate plant parameters, however, would be desirable as the accuracy of the estimated neural controller signals depends on the validity of the oculomotor plant parameters, which can be expected to vary to some degree between subjects [22]. For successful signal separation and estimation of the kinematic signals though, moderate model mismatches are unproblematic as they are compensated by the estimated neural controller signals. A further limitation is that the MBSDC framework works with a one-dimensional model and is currently specifically tailored to horizontal eye movements. A promising extension would be to replace the oculomotor plant for horizontal eye movements with a 2D [22] or even a 3D [21] oculomotor model and estimate the neural controller signals to the two or three muscle pairs jointly.

D. Computational Cost

The bulk of the computation is due to Kalman smoothing. The analysis of a 10 s recording at 1 kHz lasted 20 s using MATLAB 2017a on a MacBook Pro with an Intel Core i5 processor.

VII. Conclusion

In this paper we have proposed a model-based eye movement analysis framework. The framework builds on an established physiological model for horizontal eye movements [20], that we have extended by neural controller signals for saccades, SPEM and FEM, and with a measurement model accounting for disturbances such as blinks. To recover kinematic signals (noise-free eye position, velocity and acceleration), instead of using lowpass filters and numerical differentiation, we use state and sparse-input estimation techniques in state space models. In addition to outperforming traditional approaches, based on lowpass filtering and numerical differentiation, the proposed framework can estimate additional physical signals such as forces of the oculomotor muscles and neural controller signals. By estimating neural controller signals for saccades, SPEM and FEM, a signal separation is performed in the neural domain. The separated signals can then be analyzed independently, which opens up the possibility of analyzing multi-type eye movements as commonly encountered in free-viewing conditions. By making the code open source, we hope that the MBSDC framework will be useful for diverse eye movement analysis tasks.

Appendix

Here, we provide the theoretical background of the MBSDC framework. We cover state space models, inference algorithms such as Kalman smoothing and its generalization Gaussian message passing, as well as parameter learning algorithms, in particular the EM algorithm and its role in sparse input estimation. To describe the models and algorithms we use a type of probabilistic graphical model called a factor graph [23].

A. Probabilistic Formulation of State Space Models

We consider linear time-invariant SSMs of the form

$$X_k = AX_{k-1} + BU_k + W_k \tag{55}$$

$$Y_k = CX_k + Z_k, \tag{56}$$

with $k = 1, \ldots, L$. For Gaussian inputs U, initial state X_0, and state and observation noise, W and Z, the SSM (55)–(56) is

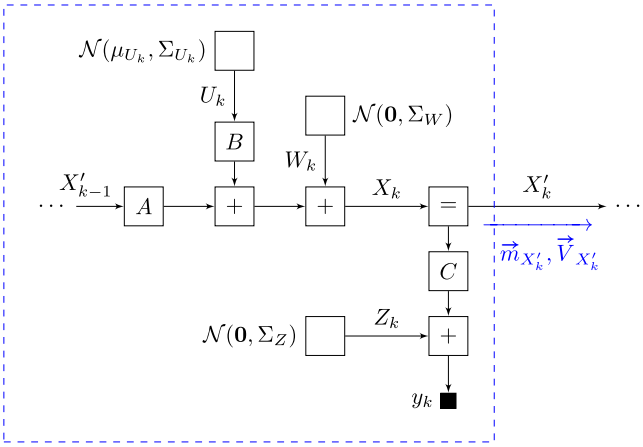

Fig. 10. Factor graph of the SSM (55)–(56). *Dashed box:* Forward mean $\vec{m}_{X'_k}$ (65) and covariance $\vec{V}_{X'_k}$ (66) of the Gaussian distribution $p(x'_k|y_1, \ldots, y_k)$ obtained by integrating over all variables inside the dashed box [23]. The black square represents an observed variable.

linear Gaussian with a joint density that factorizes as

$$p(y, x, u) = p(x_0) \prod_{k=1}^{L} p(y_k|x_k) p(x_k|x_{k-1}, u_k) p(u_k) \tag{57}$$

$$= \mathcal{N}(x_0|\mu_{X_0}, \Sigma_{X_0}) \cdot \left(\prod_{k=1}^{L} \mathcal{N}(y_k|Cx_k, \Sigma_Z) \right.$$

$$\left. \cdot \mathcal{N}(x_k|Ax_{k-1} + Bu_k, \Sigma_W) \cdot \mathcal{N}(u_k|\mu_{U_k}, \Sigma_{U_k}) \right). \tag{58}$$

This density is represented by the factor graph in Fig. 10.

B. Inference in SSMs – Gaussian Message Passing

In linear Gaussian SSMs, inference, i.e., the computation of the posterior distributions

$$p(x_k|y) = \mathcal{N}(x_k|m_{X_k}, V_{X_k}) \tag{59}$$

$$p(u_k|y) = \mathcal{N}(u_k|m_{U_k}, V_{U_k}), \tag{60}$$

amounts to the computation of the mean vectors and covariance matrices of X_k and U_k. These can be obtained by Gaussian message passing [23]. In the forward pass (Kalman filtering) we compute the quantities

$$\vec{m}_{X_k} = A\vec{m}_{X'_{k-1}} + B\mu_{U_k} \tag{61}$$

$$\vec{V}_{X_k} = A\vec{V}_{X'_{k-1}} A^{\mathsf{T}} + B\Sigma_{U_k} B^{\mathsf{T}} + \Sigma_W \tag{62}$$

$$G_k = (\Sigma_Z + C\vec{V}_{X_k} C^{\mathsf{T}})^{-1} \tag{63}$$

$$F_k = I - \vec{V}_{X_k} C^{\mathsf{T}} G_k C \tag{64}$$

$$\vec{m}_{X'_k} = \vec{m}_{X_k} + \vec{V}_{X_k} C^{\mathsf{T}} G_k (y_k - C\vec{m}_{X_k}) \tag{65}$$

$$\vec{V}_{X'_k} = F_k \vec{V}_{X_k}, \tag{66}$$

for $k = 1, \ldots, L$, with initializations $\vec{m}_{X'_0} = \mu_{X_0}$ and $\vec{V}_{X'_0} = \Sigma_{X_0}$. The right-pointing arrows on top of the Gaussian message parameters (mean vectors and covariance matrices) refer to the fact that these are summary statistics from the left-side of the factor graph in Fig. 10. In the backward pass (Kalman smoothing) we compute [24]

$$\tilde{\xi}_{X_k} = F_k^{\mathsf{T}} A^{\mathsf{T}} \tilde{\xi}_{X_{k+1}} - C^{\mathsf{T}} G_k (y_k - C\vec{m}_{X_k}) \tag{67}$$

$$\tilde{W}_{X_k} = F_k^{\mathsf{T}} A^{\mathsf{T}} \tilde{W}_{X_{k+1}} A F_k + C^{\mathsf{T}} G_k C, \tag{68}$$

for $k = L, \ldots, 0$, with $\tilde{\xi}_{X_{N+1}}$ and $\tilde{W}_{X_{N+1}}$ initialized to all zeros, $F_0 = I$, and $G_0 = 0$. The means and variances are

$$m_{X_k} = \vec{m}_{X_k} - \vec{V}_{X_k} \tilde{\xi}_{X_k} \tag{69}$$

$$V_{X_k} = \vec{V}_{X_k} (I - \tilde{W}_{X_k} \vec{V}_{X_k}) \tag{70}$$

$$m_{U_k} = \mu_{U_k} - \Sigma_{U_k} B^{\mathsf{T}} \tilde{\xi}_{X_k} \tag{71}$$

$$V_{U_k} = \Sigma_{U_k} (I - B^{\mathsf{T}} \tilde{W}_{X_k} B \Sigma_{U_k}). \tag{72}$$

Note that (67)–(70) correspond to the (Modified-Bryson-Frazier) Kalman smoother updates, and (71)–(72) is an augmentation of this smoother to input estimation [24].

C. Learning SSM Parameters With the EM Algorithm

Learning refers to the task of estimating unknown parameters Θ, e.g., by the maximum a posteriori estimation

$$\widehat{\Theta} = \operatorname*{argmax}_{\Theta} p(\Theta|y) = \operatorname*{argmax}_{\Theta} \log(p(y|\Theta)p(\Theta)). \tag{73}$$

In SSMs, this maximization can be performed with an EM algorithm [48] with X and U as latent variables. The M-step of the EM algorithm is

$$\widehat{\Theta}^{\text{new}} = \operatorname*{argmax}_{\Theta} \mathsf{E}[\log p(y, X, U|\Theta)] + \log p(\Theta), \tag{74}$$

where the expectation is taken w.r.t. the posterior over the latent variables $p(x, u|y, \widehat{\Theta}^{\text{old}})$. Using (58) we obtain

$$\mathsf{E}[\log p(y, X, U|\Theta)]$$

$$= -\frac{1}{2} \left(\sum_{k=1}^{L} \mathsf{E} \left[\log|2\pi\Sigma_Z| + \|y_k - CX_k\|^2_{\Sigma_Z^{-1}} + \log|2\pi\Sigma_W| \right.\right.$$

$$\left.\left. + \|X_k - AX_{k-1} - BU_k\|^2_{\Sigma_W^{-1}} + \log|2\pi\Sigma_{U_k}| + \|U_k\|^2_{\Sigma_{U_k}^{-1}} \right] \right)$$

$$- \frac{1}{2} \left(\mathsf{E}[\|X_0\|^2_{\Sigma_{X_0}^{-1}}] + \log|2\pi\Sigma_{X_0}| \right) \tag{75}$$

where $\|x\|^2_A \triangleq x^{\mathsf{T}} A x$ and $|A|$ denotes the determinant of A. The second moments of X_k and U_k in (75) are readily obtained from the posterior means and variances (69)–(72). The second moments in (44) and (46) are

$$\mathsf{E}[U_k^2|y, \Theta] = V_{U_k} + m_{U_k}^2 \tag{76}$$

$$\mathsf{E}[Z_k^2|y, \Theta] = y_k^2 - 2y_k C m_{X_k} + C(V_{X_k} + m_{X_k} m_{X_k}^{\mathsf{T}}) C^{\mathsf{T}}. \tag{77}$$

D. Modeling and Estimation of Sparse Inputs

In a probabilistic setting, sparse variables $U = (U_1, \ldots, U_L)$ are modeled with sparsity-promoting priors

$$p(u) = \prod_{k=1}^{L} p(u_k), \tag{78}$$

which in the sparse Bayesian learning (SBL) framework [36] are represented via the hierarchical representation [37]

$$p(u_k) = \sup_{\sigma_k \geq 0} \mathcal{N}(u_k|0, \sigma_k^2) p(\sigma_k), \tag{79}$$

with a suitable hyperprior $p(\sigma_k)$. Note that essentially all sparsity promoting priors (Laplace, Student-t, ...) can be represented this way [36]. In SBL, instead of estimating $U = (U_1, \ldots, U_L)$ directly, we first estimate $\sigma = (\sigma_1, \ldots, \sigma_N)$ for marginalized-out U, i.e.,

$$\widehat{\sigma} = \operatorname*{argmax}_{\sigma} p(\sigma|y), \tag{80}$$

and then obtain an estimate of U by

$$\widehat{u} = \mathsf{E}[U|y, \widehat{\sigma}]. \tag{81}$$

Note that (80) is a learning problem of the form (73) and can be solved by EM (Appendix C). In our MBSDC framework in (79) we use the hyperprior

$$p(\sigma_k|\alpha, \beta) \propto \sigma_k^{-\alpha} \exp(-\beta/\sigma_k). \tag{82}$$

In Appendix E we discuss how to choose the hyperparameters $\alpha \geq 0$ and $\beta \geq 0$.

E. Relevant Parameters in the MBSDC Framework

In the following we discuss the most relevant parameters.

1) Observation Noise Estimation: The observation noise level σ_{Noise} controls the trade-off between model-fit and regularization. The maximum a posteriori estimate of σ_{Noise} is obtained by an EM-algorithm. The hyperparameter α_{Noise} in (46) controls the prior on σ_{Noise}, where $\alpha_{\text{Noise}} = 0$ corresponds to maximum-likelihood estimation, and $\alpha_{\text{Noise}} > 0$ introduces a bias towards smaller values of σ_{Noise}.

2) Sparse Input Estimation: The sparsity of U^{Sacc} and U^{Blink} are controlled by α_{Sacc} and α_{Blink}. Larger values of these parameters result in sparser estimates. We used values between 0.3 and 1 for α_{Sacc}, and between 6 and 10 for α_{Blink}. The parameters β_{Sacc} and β_{Blink} control the number of EM-iterations and are chosen to be small (e.g., $\beta_{\text{Sacc}} = \beta_{\text{Blink}} = 10^{-6}$). To achieve true sparsity, we set all variances below $20 \cdot \beta_{\text{Sacc}}$ (and $20 \cdot \beta_{\text{Blink}}$, respectively) to zero.

3) SPEM Estimation: The variance σ^2_{SPEM} of the Gaussian prior on the SPEM input signal U^{SPEM} in (1) determines how quickly the SPEM signal Y^{SPEM} is allowed to change. We used values between $\sigma_{\text{SPEM}} = 0$ N/s^2 (no SPEM) and 1 N/s^2.

4) FEM Estimation: The FEM input variance σ^2_{FEM} should be adapted to the expected amount of FEM in the data. We used values between $\sigma_{\text{FEM}} = 0$ N/s and 1 N/s. For too small values, FEMs in the data might be explained by the saccade neural controller signal and for too large values, small saccades might be missed and explained by the FEM signal.

References

[1] R. J. Leigh and D. S. Zee, *The Neurology of Eye Movements*, 5th ed. New York, NY, USA: Oxford Univ. Press, 2015.

[2] J. E. Silberg *et al.*, "Free visual exploration of natural movies in schizophrenia," *Eur. Arch. Psychiatry Clin. Neurosci.*, vol. 269, no. 4, pp. 407–418, Jun. 2019.

[3] K. Srulijes *et al.*, "Association between vestibulo-ocular reflex suppression, balance, gait, and fall risk in ageing and neurodegenerative disease: Protocol of a one-year prospective follow-up study," *BMC Neurol.*, vol. 15, Oct. 2015, Art. no. 192.

[4] A. L. Yarbus, *Eye Movements and Vision*, 1st ed. Boston, MA, USA: Springer, 1967.

[5] T. Eggert, "Eye movement recordings: Methods," *Dev. Ophthalmol.*, vol. 40, pp. 15–34, Feb. 2007.

[6] P. Inchingolo and M. Spanio, "On the identification and analysis of saccadic eye movements—A quantitative study of the processing procedures," *IEEE Trans. Biomed. Eng.*, vol. BME-32, no. 9, pp. 683–695, Sep. 1985.

[7] M. Juhola, "The effect of digital lowpass filters on the maximum velocity of saccadic eye movements," *Comput. Biol. Med.*, vol. 16, no. 5, pp. 361–370, Dec. 1986.

[8] D. J. Mack, S. Belfanti, and U. Schwarz, "The effect of sampling rate and lowpass filters on saccades—A modeling approach," *Behav. Res. Methods*, vol. 49, no. 6, pp. 2146–2162, Jan. 2017.

[9] D. Salvucci and J. Goldberg, "Identifying fixations and saccades in eye-tracking protocols," in *Proc. Symp. Eye Tracking Res. Appl.*, Palm Beach Gardens, Florida, USA, Nov. 2000, pp. 71–78.

[10] C. M. Harris, J. Wallman, and C. A. Scudder, "Fourier analysis of saccades in monkeys and humans," *J. Neurophysiol.*, vol. 63, no. 4, pp. 877–886, Apr. 1990.

[11] Y. Ebisawa *et al.*, "New methods for removing saccades in analysis of smooth pursuit eye movement," *Biol. Cybern.*, vol. 60, no. 2, pp. 111–119, Dec. 1988.

[12] J. Pekkanen and O. Lappi, "A new and general approach to signal denoising and eye movement classification based on segmented linear regression," *Sci. Rep.*, vol. 7, Dec. 2017, Art. no. 17762.

[13] R. Zemblys *et al.*, "Using machine learning to detect events in eye-tracking data," *Behav. Res. Methods*, vol. 50, no. 1, pp. 160–181, Feb. 2017.

[14] R. Zemblys, D. C. Niehorster, and K. Holmqvist, "Gazenet: End-to-end eye-movement event detection with deep neural networks," *Behav. Res. Methods*, vol. 51, no. 2, pp. 840–864, Apr. 2019.

[15] I. T. C. Hooge *et al.*, "Is human classification by experienced untrained observers a gold standard in fixation detection?" *Behav. Res. Methods*, vol. 50, no. 5, pp. 1864–1881, Oct. 2018.

[16] R. S. Hessels *et al.*, "Is the eye-movement field confused about fixations and saccades? A survey among 124 researchers," *Roy. Soc. Open Sci.*, vol. 5, no. 8, 2018, Art. no. 180502.

[17] D. A. Robinson, "The mechanics of human saccadic eye movement," *J. Physiol.*, vol. 174, no. 2, pp. 245–264, Nov. 1964.

[18] A. T. Bahill, "Development, validation and sensitivity analysis of human eye movement models," *CRC Crit. Rev. Bioeng.*, vol. 4, no. 4, pp. 311–355, Dec. 1980.

[19] J. Enderle, *Models of Horizontal Eye Movements, Part I: Early Models of Saccades and Smooth Pursuit*. San Rafael, CA, USA: Morgan & Claypool, 2010.

[20] W. Zhou, X. Chen, and J. Enderle, "An updated time-optimal 3rd-order linear saccadic eye plant model," *Int. J. Neural Syst.*, vol. 19, no. 5, pp. 309–330, Oct. 2009.

[21] W. Zhou *et al.*, "Dynamic characteristics of a new three-dimensional linear homeomorphic saccade model," *Int. J. Neural Syst.*, vol. 28, no. 3, pp. 50–69, Oct. 2018.

[22] O. Komogortsev *et al.*, "2D linear oculomotor plant mathematical model: Verification and biometric applications," *ACM Trans. Appl. Perception*, vol. 10, no. 4, Oct. 2013, Art. no. 27.

[23] H.-A. Loeliger *et al.*, "The factor graph approach to model-based signal processing," *Proc. IEEE*, vol. 95, no. 6, pp. 1295–1322, Jun. 2007.

[24] H.-A. Loeliger *et al.*, "On sparsity by NUV-EM, Gaussian message passing, and Kalman smoothing," in *Proc. Inf. Theory Appl. Workshop*, Jan. 2016, pp. 1–10.

[25] F. Wadehn *et al.*, "Estimation of neural inputs and detection of saccades and smooth pursuit eye movements by sparse Bayesian learning," in *Proc. Annu. Int. Conf. IEEE Eng. Med. Biol. Soc.*, Honolulu, HI, USA, Jul. 2018, pp. 2619–2622.

[26] R. Dodge, "Five types of eye movements in the horizontal meridian plane of the field of regard," *J. Physiol.*, vol. 8, pp. 307–329, Jan. 1903.

[27] A. J. Peltsch *et al.*, "Age-related trends in saccade characteristics among the elderly," *Neurobiol. Aging*, vol. 32, no. 4, pp. 669–679, Apr. 2011.
[28] D. J. Mack and U. J. Ilg, "The effects of video game play on the characteristics of saccadic eye movements." *Vision Res.*, vol. 102, pp. 26–32, Sep. 2014.
[29] R. Anderson and M. R. MacAskill, "Eye movements in patients with neurodegenerative disorders," *Nature Rev. Neurol.*, vol. 9, no. 2, pp. 74–85, Jan. 2013.
[30] D. S. Zee *et al.*, "Slow saccades in spinocerebellar degeneration," *Arch. Neurol.*, vol. 33, no. 4, pp. 243–251, Apr. 1976.
[31] M. T. Avila *et al.*, "Role of anticipation in schizophrenia-related pursuit initiation deficits," *J. Neurophysiol.*, vol. 95, no. 2, pp. 593–601, Feb. 2006.
[32] Y. Takarae *et al.*, "Pursuit eye movement deficits in autism," *Brain*, vol. 127, no. 12, pp. 2584–2594, Dec. 2004.
[33] G. T. Gitchel, P. A. Wetzel, and M. S. Baron, "Pervasive ocular tremor in patients with Parkinson disease," *Arch. Neurol.*, vol. 69, no. 8, pp. 1011–1017, Aug. 2012.
[34] U. J. Ilg, "Slow eye movements," *Prog. Neurobiol.*, vol. 53, no. 3, pp. 293–329, Oct. 1997.
[35] G. F. Franklin, J. Powell, and M. Workman, *Digital Control of Dynamic Systems*, 3rd ed. Half Moon Bay, CA, USA: Ellis-Kagle, 1998.
[36] M. Tipping, "Sparse Bayesian learning and the relevance vector machine," *J. Mach. Learn. Res.*, vol. 1, pp. 211–244, Jun. 2001.
[37] H.-A. Loeliger *et al.*, "Factor graphs with NUV priors and iteratively reweighted descent for sparse least squares and more," in *Proc. Int. Symp. Turbo Codes Iterative Inform. Process.*, Hong Kong, Dec. 2018, pp. 1–5.
[38] D. L. Sparks, "The brainstem control of saccadic eye movements," *Nature Rev. Neurosci.*, vol. 3, no. 1, pp. 952–964, Dec. 2002.
[39] P. Thier and U. J. Ilg, "The neural basis of smooth-pursuit eye movements," *Curr. Opin. Neurobiol.*, vol. 15, no. 6, pp. 645–652, Nov. 2005.
[40] L. Larsson, M. Nyström, and M. Stridh, "Detection of saccades and post-saccadic oscillations in the presence of smooth pursuit," *IEEE Trans. Biomed. Eng.*, vol. 60, no. 9, pp. 2484–2493, Sep. 2013.
[41] A. T. Bahill and L. Stark, "Overlapping saccades and glissades are produced by fatigue in the saccadic eye movement system," *Exp. Neurol.*, vol. 48, no. 1, pp. 95–106, 1975.
[42] M. Prsa, P. W. Dicke, and P. Thier, "The absence of eye muscle fatigue indicates that the nervous system compensates for non-motor disturbances of oculomotor function," *J. Neurosci.*, vol. 30, no. 47, pp. 834–842, Nov. 2010.
[43] U. J. Ilg, Schülerlabor Neurowissenschaften. [Online]. Available: www.neuroschool-tuebingen-schuelerlabor.de. Accessed: Jan. 2018. https://www.cin.uni-tuebingen.de/about-cin/people/cin-members/person-detail/prof-dr-uwe-ilg.html
[44] C. M. Harris and D. M. Wolpert, "The main sequence of saccades optimizes speed-accuracy trade-off," *Biol. Cybern.*, vol. 95, no. 1, pp. 21–29, Jul. 2006.
[45] R. Andersson *et al.*, "One algorithm to rule them all? An evaluation and discussion of ten eye movement event-detection algorithms," *Behav. Res. Methods*, vol. 49, no. 2, pp. 616–637, Apr. 2017.
[46] J. R. Tregellas *et al.*, "Neurobiology of smooth pursuit eye movement deficits in schizophrenia: An FMRI study," *Amer. J. Psychiatry*, vol. 161, no. 2, pp. 315–321, Feb. 2004.
[47] A. J. van Opstal and H. Goossens, "Linear ensemble-coding in midbrain superior colliculus specifies the saccade kinematics," *Biol. Cybern.*, vol. 98, no. 6, pp. 561–577, Jun. 2008.
[48] R. H. Shumway and D. S. Stoffer, "An approach to time series smoothing and forecasting using the EM algorithm," *J. Time Series Anal.*, vol. 3, no. 4, pp. 253–264, Jul. 1982.